Author(s): Abdelhalim, Walaa Ali; Rabee, Ahmed R.; Soliman, Saied M.; Hagar, Mohamed; Moneer, Esraa A.; Bakr, Basant A.; Barakat, Assem; Haukka, Matti; Rasheed, Hanaa A.

Title: New formyl indole derivatives based on thiobarbituric acid and their nano-formulations : synthesis, characterization, parasitology and histopathology investigations

Year: 2025

Version: Published version

Please cite the original version:

Abdelhalim, W. A., Rabee, A. R., Soliman, S. M., Hagar, M., Moneer, E. A., Bakr, B. A., Barakat, A., Haukka, M., & Rasheed, H. A. (2025). New formyl indole derivatives based on thiobarbituric acid and their nano-formulations : synthesis, characterization, parasitology and histopathology investigations. Scientific Reports, 15, Article 299. https://doi.org/10.1038/s41598-024-81683-6

scientific reports

Check for updates

OPEN

New formyl indole derivatives based on thiobarbituric acid and their nano-formulations; synthesis, characterization, parasitology and histopathology investigations

Walaa Ali Abdelhalim[1], Ahmed R. Rabee[1]✉, Saied M. Soliman[1]✉, Mohamed Hagar[1]✉, Esraa A. Moneer[2], Basant A. Bakr[3], Assem Barakat[4], Matti Haukka[5] & Hanaa A. Rasheed[1]

New formyl indole derivatives based on thiobarbituric acid were designed for targeting parasitological applications. The new compounds (5-((1*H*-indol-3-yl)methylene)-2-thioxodihydropyrimidine-4,6(1*H*,5*H*)-dione (3a), and 5-((1-benzyl-1*H*-indol-3-yl)methylene)-2-thioxodihydropyrimidine-4,6(1*H*,5*H*)-dione (3b) were synthesized as thioxodihydropyrimidine derivatives *via* aldol condensation reaction. The structures of the synthesized compounds were confirmed based on their spectral data *via* FT-IR, ^{1}H and ^{13}C NMR spectral characterization. In addition, the structure of 3a is confirmed using X-ray crystallography. The synthesized compounds were prepared in nm scale *via* chitosan as a matrix, and their size was measured *via* scanning electronic microscope. Interestingly, the newly synthesized nano formulations show higher positive zeta potential (mV) values + 29.6 and + 26.1 for compounds NP-3a, and NP-3b; respectively. These compounds were tested for their parasitological activity. The results revealed that 3b had a great activity against cryptosporidium infection. Moreover, the nano formulation of compound 3b showed a significant reduction percent of oocyst count of cryptosporidium infected mice representing 66%. Furthermore, these compounds were screened by in-vitro hemolytic activity assay (IC_{50}) values (cytotoxicity on RBCs) to assess their cytotoxic potentials and safety profiles.

Keywords Thiobarbituric acid, Aldol condensation, Nano formulation, Parasitology, Histopathology investigation

Heterocyclic compounds are crucial organic systems utilized in several sectors owing to their ability to treat multiple diseases, such as chalcone derivatives as acetylcholinesterase inhibitors[1–3]. One of the natural heterocyclic compounds is indole which has a bicyclic structure and could concern a prevalent position through heterocycles in drug invention[4]. It could be obtained from organic synthesis or isolated from natural products like jasmine, orange blossom, and tuberose. These heterocyclic ring systems are important origin of pharmacologically active compounds[5,6]. They generally act as hydrogen bond acceptors and donors. Accordingly, they could bind to biological targets among intermolecular hydrogen bonds successfully[5].

Indoles include widely studied heterocyclic compounds for various fields of application in pathophysiological conditions[7], anti-cancer[8–11], anti-microbial[12], anti-inflammatory[13], anti-viral[14]infections, migraine, depression, hypertension and emesis. In addition, to its applications in drug research, It has several applications in many sectors such as agrochemicals[15], perfumery as it has a strong smell that can be pleasant in low concentrations and industries such as cosmetics, solvents, and antioxidants[16].

[1]Chemistry Department, Faculty of Science, Alexandria University, P.O. Box 426, Alexandria 21321, Egypt. [2]Department of Medical Laboratory Technology, Faculty of Applied Health Sciences Technology, Pharos University in Alexandria, Alexandria 21500, Egypt. [3]Department of Zoology, Faculty of Science, Alexandria University, Alexandria, Egypt. [4]Department of Chemistry, College of Science, King Saud University, P. O. Box 2455, Riyadh 11451, Saudi Arabia. [5]Department of Chemistry, University of Jyväskylä, P.O. Box 35, Jyväskylä FI-40014, Finland. ✉email: ahmedrabee@alexu.edu.eg; ahmedramadanrabee@gmail.com; Saeed.soliman@alexu.edu.eg; saied1soliman@yahoo.com; mohamed.hagar@alexu.edu.eg; mohamedhaggar@gmail.com

On the other hand, thiobarbituric acid (TBA) can react with several reagents to form a large class of hybrid heterocyclic compounds, like pyrimidine derivatives and indolyl derivatives[17–19]. In addition, TBA can be used as a reducing agent in photographic developers[20]. It could also act as a reagent in some biochemical assays such as measuring lipid peroxidation[21]. TBA differs from barbituric acid in the location of the sulfur instead of carbonyl oxygen at the C-2 position and this difference provides TBA high solubility in lipids[22].

Thiobarbituric acid has an active methylene carbon that serves as the main precursor used in the Knoevenagel condensation[23–26]. Presently, the development of synthetic methodologies poses great challenges to organic chemists. This is due to the presence of compounds with active methylene groups that have multilateral organic precursors with special chemical reactivity. Whereas active methylene compounds exhibit specific reactions to the functional groups attached to the methylene group. They also exhibit a highly acidic hydrogen-dependent reaction towards the active methylene group[27].

The unicellular apicomplexan protozoan parasites known as Cryptosporidium species infect humans and many other animals[28]. Usually, the face-oral route of infection is contracted by consuming water or food tainted by the oocyst[29]. Cryptosporidium parvum (C. parvum) and Cryptosporidium hominis are the most commonly found human infection species[30]. The immune system plays a crucial part in preventing and managing cryptosporidiosis[31]. Therefore, immunocompromised patients often have a chronic, deadly illness, whereas immunocompetent people just have a self-limited illness[32]. NTZ is the only medication licensed by the Food and Drug Administration to treat cryptosporidiosis. Although NTZ was a significant advancement in the treatment of cryptosporidiosis in kids, its poor effectiveness in immunocompromised and starving persons highlighted the need for improved medications for cryptosporidiosis therapy[33].

Therefore, the alkylation of thiobarbituric acid and its benzylidene derivatives have attracted the attention of researchers in medicinal chemistry and therapeutic medications, and pharmacologic action and some of them are more important due to their several biological activities[34]. In this work, new formyl indole derivatives were prepared from thiobarbituric acid derivatives *via*aldol condensation for their application as anti-parasites and discuss their histopathological investigation. Chitosan nanoparticles encapsulated with these bioactive molecules were used for the biological experiments since such methodology could provide controlled release ensuring a sustained therapeutic effect[35].

Results and discussion

Chemistry

Two new formyl indole derivatives based on thiobarbituric acids *via* aldol condensation were obtained as adopted in Scheme 1. Aldol condensation of the thiobarbituric acid **1** with formyl indole derivatives (**2a** or **2b**) in presence of ethanol and glacial acetic acid under reflux furnished the corresponding thioxodihydropyrimidine derivatives (**3a** or **3b**) in a high yield.

The structure of the synthesized compounds **3a** and **3b** was confirmed using spectroscopic data. The structure of compound **3a** was confirmed by its IR spectrum which showed strong band at 3437 cm^{-1} corresponds to **N-H** stretch, 1636 cm^{-1} for (**C=O**) stretch, 1533 cm^{-1} (**C=C**) and 1062 cm^{-1} for (**C=S**). The ^{1}HNMR spectrum showed broad singlet band at δ = 12.90 ppm for NH indole proton, doublet signal at δ = 12.21 and 12.16 ppm corresponding to 2 H for NH of thiobarbituric acid protons. A singlet signal at δ = 9.54 ppm was assigned to the aldehydic proton of the DMF incorporated in the crystal lattice. In addition, the X-ray structure of **3a** is reported and found in good agreement with the spectral characterization (Fig. 1). The structure of compound **3b** was confirmed by its IR spectrum which showed bands at 3437 cm^{-1}, 1635 cm^{-1}, 1531 cm^{-1}, 1061 cm^{-1} for (NH), (**C=O**), (C=C) and (C=S) respectively.

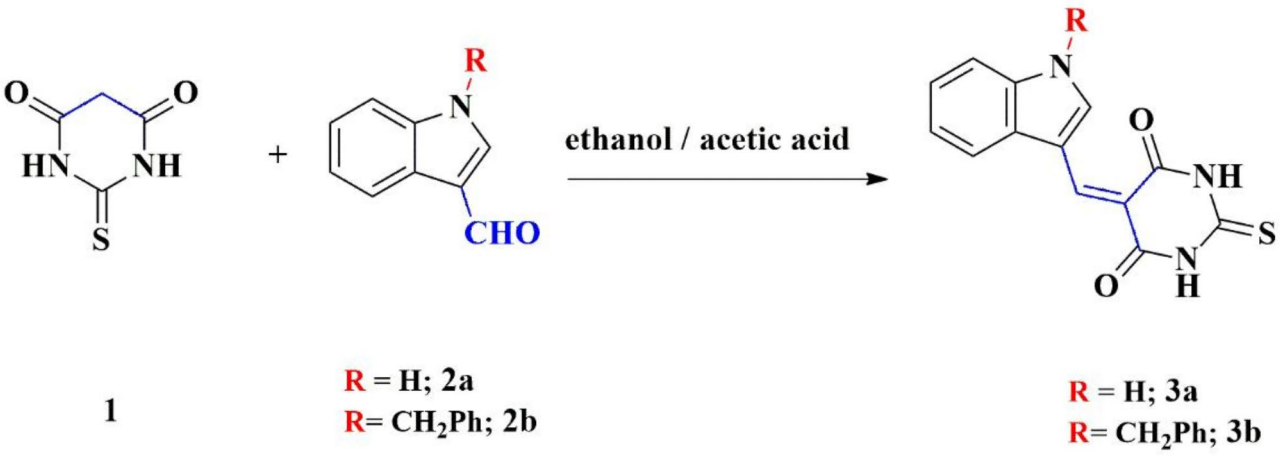

Scheme 1. Synthesis of thioxo dihydro pyrimidine derivatives.

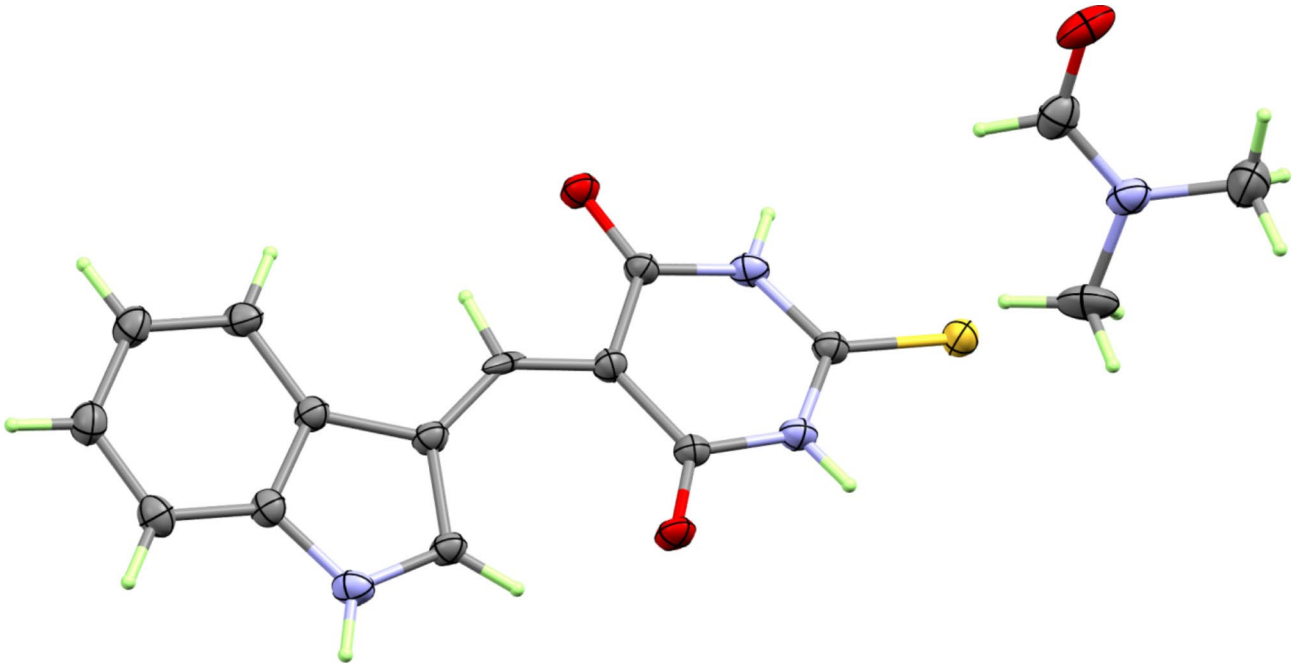

Fig. 1. X-ray structure of **3a.**

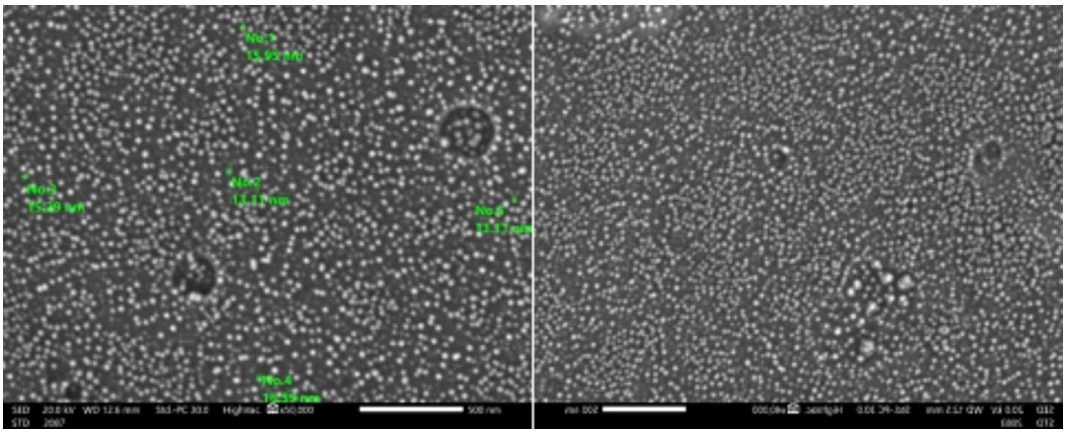

Fig. 2. SEM images for nanocrystals of compound **3a**.

Nano formulation of the synthesized compounds

Our work is focused on the preparation of compounds **3a** and **3b** on the nanometer scale *via*the ionic gelation method using chitosan nanoparticles. Nano formulation allows for unique physicochemical properties that can enhance the efficacy and bioavailability of therapeutic agents. The nanoparticles have a wide range of specifications such as enhanced solubility and activities. The size of the prepared nanoparticles was measured utilizing a scanning electronic microscope[36] and the particle size was found in a range of 10–15 nm (Figs. 2, 3, 4 and 5), and the polydispersity index (PDI) of nanoparticles **3a** and **3b** are 0.537 and 0.664, respectively. Both compound **3a** and **3b** possess high positive zeta potential + 29.6, + 26.1, respectively as tabulated in Tables 1 and 2.

Biological evaluation

Cytotoxic effects on RBCs

The in vitro cytotoxic effects on RBCs of compounds **3a** and **3b** were assessed using hemolytic activity was showed in Fig. 6. It was found that, the hemolysis percentages were 28.75 and 26.67% at 80 µg/mL for compounds **3a**, and **3b**, respectively while theIC_{50} values are 139.13 ± 0.05 and 150.00 ± 0.03, respectively.

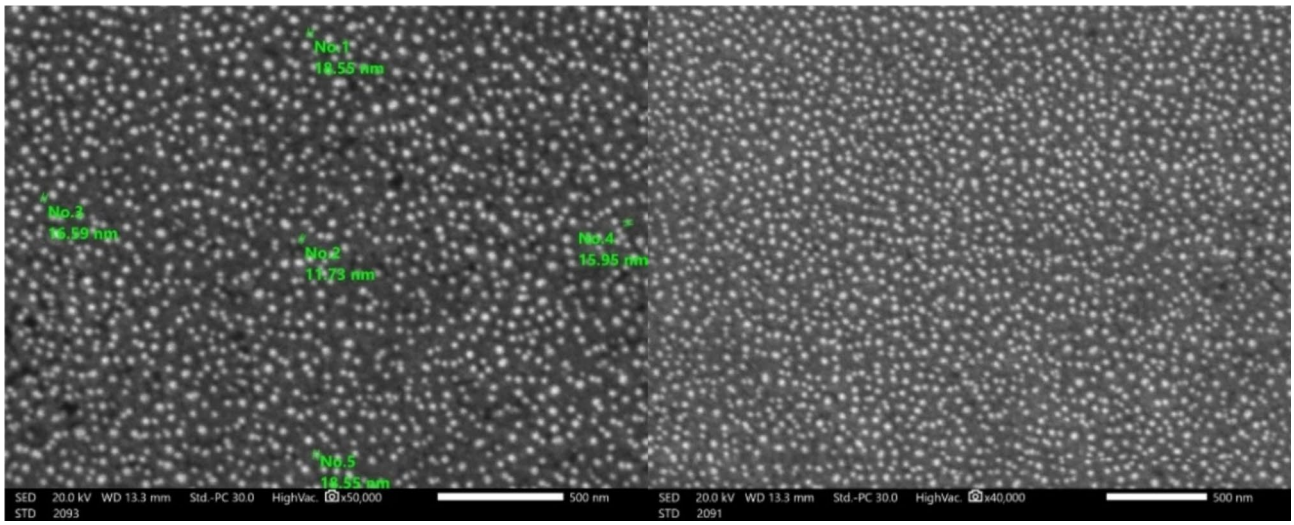

Fig. 3. SEM images for nanocrystals of compound **3b**.

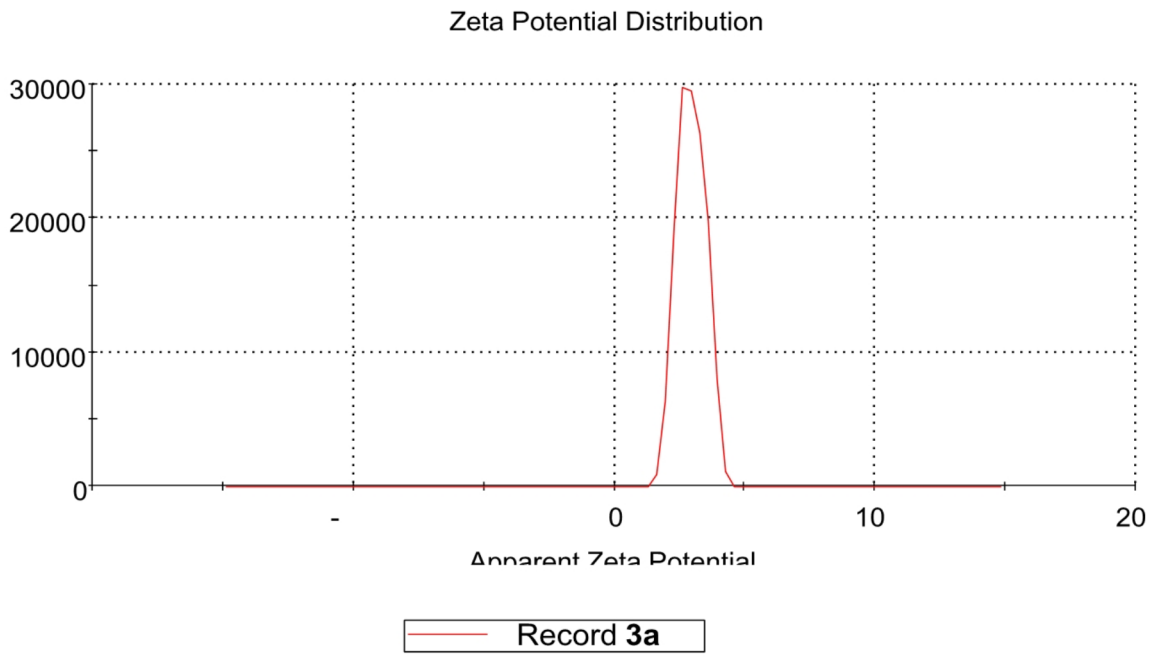

Fig. 4. Zeta potential distribution curve for compound **3a**.

Parasitological results

The oocysts were seen using the modified Ziehl-Nelsen stain method as spherical bodies or ovals of pink vivid rose on a blue background (Fig. 7).

Table 3 The high significant statistical differences between all groups. The mean oocyst count in untreated infected group was 32.7 ± 0.9, while the mean oocyst counts in infected treated groups were 10.5 ± 0.7, 13.2 ± 1.2 and 14.8 ± 0.8 for NTZ treated group, compound **3b** treated group and compound **3a** treated group, respectively.

The highest percentages reduction of the oocyst's counts was noticed in infected treated NTZ mice group (68%) followed by nano compound **3b** treated group (66%) then compound **3b** treated group (59%).

Ultrastructure study

SEM was used to assess the ultrastructural morphological characteristics of the oocysts in the fecal sample for every group under study. While cysts retrieved from treated animals showed varying degrees of morphological alterations, oocysts from the control group appeared to be typical spherical oocysts with a regular cyst surface (Fig. 8).

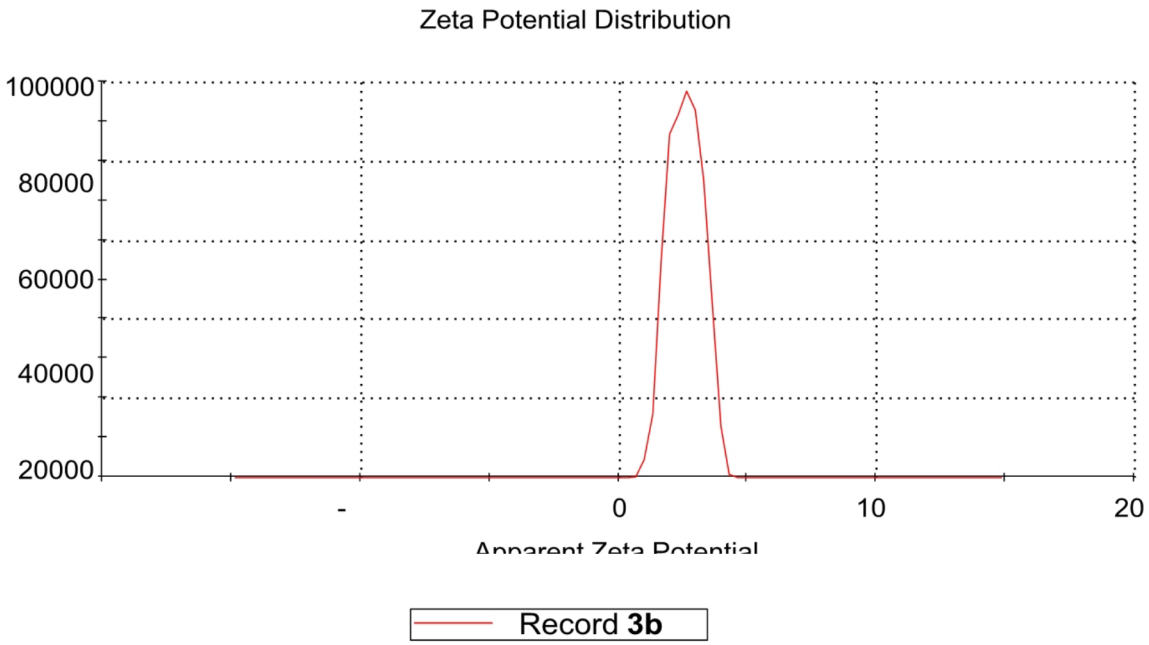

Fig. 5. Zeta potential distribution curve for compound **3b**.

			Mean (mV)	Area (%)	St Dev (mV)
Zeta Potential (mV):	**29.6**	**Peak 1**:	**29.6**	100.0	5.38
Zeta Deviation (mV):	5.38	**Peak 2**:	0.00	0.0	0.00
Conductivity (mS/cm): Result quality:	0.0240 Good	Peak 3:	0.00	0.0	0.00

Table 1. Zeta potential result of **3a**.

			Mean (mV)	Area (%)	St Dev (mV)
Zeta Potential (mV):	**26.1**	**Peak 1**:	**26.1**	100.0	6.60
Zeta Deviation (mV):	6.60	**Peak 2**:	0.00	0.0	0.00
Conductivity (mS/cm): Result quality:	0.0318 Good	Peak 3:	0.00	0.0	0.00

Table 2. Zeta potential result of **3b**.

Histopathology investigations

The negative control group's intestinal structure demonstrated normal layers (villi, submucosa, outer and inner muscularis layers, and serosa); moreover, the villi showed normal relative length, many goblet cells, and a normal lymphocyte ratio (Fig. 9(**A**, **a**)).

The positive control group, which was infected with Cryptosporidium spp., had total degeneration of the muscularis and serosa layers, in contrast to the previously indicated findings. It showed notable shrinkage of the villi with sloughing tips and inflammation of the lymphatic vessels with lymphocyte absence (Fig. 9(**B**, **b**)).

With the exception of a few indications of cellular infiltration between villi, the Nan Group (treated with nitazoxanid) showed regeneration of the muscularis layer and pointed, elongated villi (Fig. 9(**C**, **c**)).

The T1 group's results showed that all intestinal layers had recovered, demonstrating its effectiveness against Cryptosporidium species. The villi still have a significant amount of inflammation, but they also showed typical columnar epithelia with plenty of goblet cells and few lymphocytes (Fig. 9(**D**, **d**)).

The T1NPs-treated group showed reduced inflammation across the villi than the T1 group, demonstrating the effectiveness of the nanoparticles. (Fig. 9(**E**, **e**))

T2 group exhibited comparable description to the previous group in a description like the standard drug, especially in Lieberkuhn's crypt, The epithelial cells' brush boundary is present in the villi structure, and the villi are thickened and flattened. (Fig. 9(**F**, **f**))

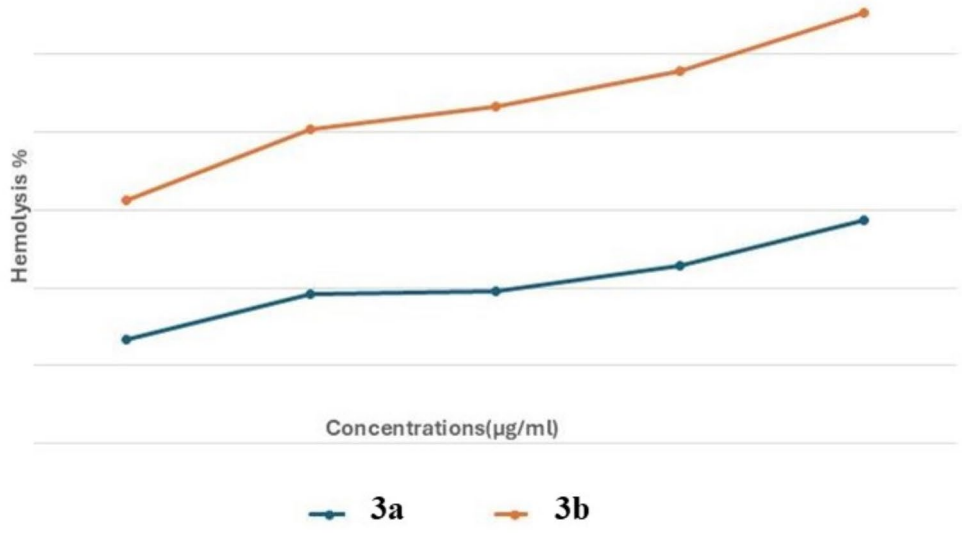

Fig. 6. The percentage of RBCs hemolysis of compounds **3a** and **3b** at different levels of concentrations.

Furthermore, the T2 group had a much higher number of crypts than the prior group, suggesting the greatest histoarchitecture outcomes. (Fig. 9(**G**, **g**))

(A, **a): negative control** presenting normal histological structure; **(B**, **b): positive control group** presenting, degenerated villi (black arrow), inflammation(red arrow) degenerated muscularized layer (double black arrow) and degeneration of crypts of Lieberkühn (black asterisk); **(C**, **c): Nan group** showing normal thickness of muscularized layer (double black arrow) normal villi (black head arrow) and inflammation (red arrow); **(D**, **d): T1 group** showing relative thickness of muscularized layer (double black arrow) normal villi (black head arrow) and inflammation (red arrow); **(E**, **e): T1-NPs group** showing thickness of muscularized layer (double black arrow) normal villi (black head arrow) and few signs of inflammation (red arrow); **(F**, **f):T2 group** showing relative thickness of muscularized layer (double black arrow) normal villi (black head arrow) with numerous goblet cells. **(G**, **g):T2-NPs group** showing muscularized layer (double black arrow) normal villi (black head arrow) with numerous goblet cells.

Materials and methods

Materials and equipment

The material and equipment characterization are reported in the supporting information.

Chemistry

*(5-((1H-indol-3-yl) methylene)−2-thioxodihydropyrimidine-4,6(1H,5H)-dione (***3a***)*

A mixture of 2-thioxodihydro pyrimidine-4,6(1*H*,5*H*)-dione (**1**) (0.01 mol) and indole-3-carbaldehyde (0.01 mol) in 30 ml of absolute ethanol and drops of acetic acid was refluxed for 12 h, the excess solvent was separated under reduced pressure then the residue was poured into cold water (200 ml). The obtained solid was filtered off then re-dissolved in EtOH/DMF (3:1 v/v) mixture. This solution is left to evaporate at room temperature to give compound **3a** as orange crystals (72% yield); $R_f = 0.44$ (n-Hexane : ethyl acetate, 1:3, V/V); m.*p* = 279–280°C; IR(KBr) νmax (cm − 1): 3437 (N-H) stretch, 1636(C = O), 1533(C = C), 1062(C = S) were observed as strong bands; 1 H NMR (500 MHz, DMSO-d6) δH: 12.90 (s, 1 H, **NH**), 12.22 (s, 1 H, **NH**), 12.16 (s, 1 H, **NH**), 9.54 (s, 1 H, CHO-DMF), 8.68 (s, 1 H, C = **CH**), 7.90 (s, 1 H, C = **CH** of indole), 7.84 (dd, J = 3.0 Hz, J = 6.0 Hz, 1 H, Ar-H), 7.56 (dd, J = 3.0 Hz, J = 6.0 Hz, 1 H, Ar-H), 7.29 (dd, J = 3.0 Hz, J = 5.0 Hz, 2 H, Ar-H), 2.83 (s, 3 H, **CH**$_3$-DMF), 2.67 (s, 3 H, **CH**$_3$-DMF); 13 C NMR (125 MHz, DMSO-d6) δC: 178.2 (C = S), 163.3, 162.8(C = O), 161.5, 145.0, 141.6, 137.1, 129.5, 124.5, 123.6, 118.3, 113.9, 112.9, 109.2 (Ar-**C**), 36.2, 31.2.

*5-((1-benzyl-1H-indol-3-yl) methylene)−2-thioxodihydropyrimidine − 4,6(1H,5H)-dione (***3b***)*

A mixture of 2-thioxodihydropyrimidine-4,6(1*H*,5*H*)-dione (**1**) (0.01 mol) and 1-benzyl-1*H*-indole-3-carbaldehyde (0.01 mol) in 30 ml of absolute ethanol and drops of acetic acid was refluxed for 12 h, the excess solvent was separated under reduced pressure then the residue was poured into cold water (200 ml). The obtained solid was filtered off and crystallized from ethanol and DMF to give compound **3b** as orange powder (68% yield); $R_f = 0.45$ (n-Hexane : ethyl acetate, 1:3, V/V); m.*p* = 309–311°C; IR(KBr) νmax (cm − 1): 3437 (N-H) stretch,

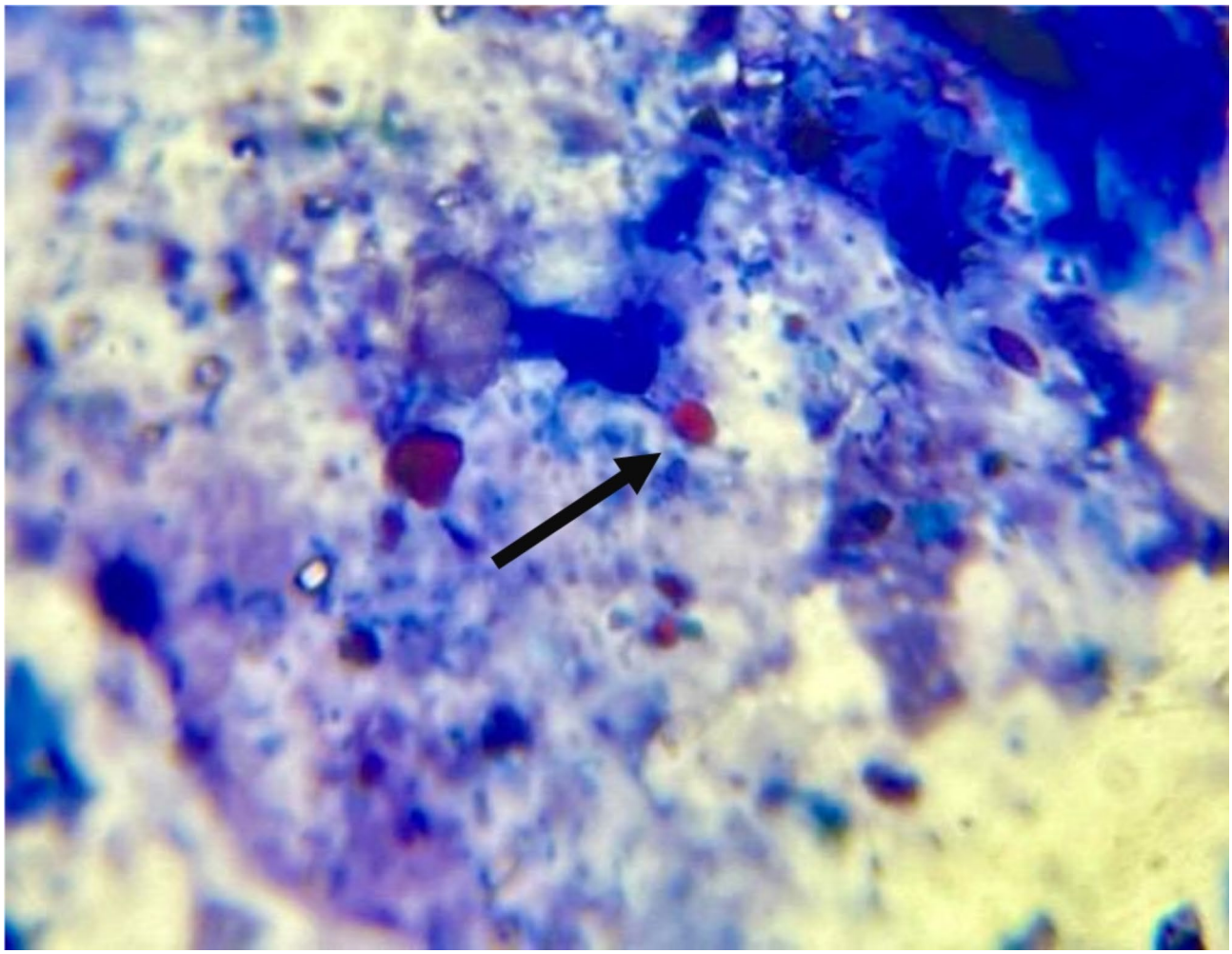

Fig. 7. Fecal smear stained with modified Ziehl–Nelsen stain viewing Cryptosporidium oocysts (black arrows) (X1000).

Shed oocysts/mg	G II	G III	G IV	G V	G VI	G VII	F	*P*
Mean ± SD	32.7 ± 0.9	10.5 ± 0.7	13.2 ± 1.2	14.8 ± 0.8	11 ± 0.8	13.3 ± 0.5	260.106	0.000
(R%)		68%	60%	55%	66%	59%		
P within groups		P1 0.000*	P2 0.000*	P3 0.000*	P4 0.000*	P5 0.000*		
			P6 0.000*	P7 0.000*	P8 0.000*	P9 0.000*		
					P110.000*	P12 0.000*		
				P10 0.000*	P13 0.000*	P14 0.000*		
						P15 0.000*		

Table 3. Comparisons of the various study groups regarding to the number of Cryptosporidium oocysts shedding immunosuppressed mice. F: One way ANOVA test, P1: GII versus GIII, P2: GII versus GIV, P3: GV versus GII, P4: GVI versus G II, P5: GVII versus GII, P6: GIV versus GIII, P7: G V versus GIII, P8: GVI versus GIII, P9: G VII versus GIII, P10: G V versus GVI, P11: G VI versus GIV , P12: GVII versus GIV, P13: GVI versus GV, P14: GVII versus GV, P15: GVII versus GVI. * p value < 0.01 significant

1635(C = O), 1531(C = C), 1061(C = S) were observed as strong bands; 1 H NMR (500 MHz, DMSO-d6) δH: 12.21 (s, 2 H, **NH**), 9.67 (d, J = 4.5 Hz, 1 H, CHO-DMF), 8.65 (d, J = 4.5 Hz, 1 H C = **CH**), 7.91 (d, J = 4.0 Hz, 1 H, C = **CH** of indole), 7.88 (d, J = 4.5 Hz, 1 H, Ar-H), 7.67 (d, J = 5.5 Hz, 1 H, Ar-H), 7.22–7.33 (m, 8 H, Ar-H), 5.67 (d, J = 3.0 Hz, 2 H, -$\mathbf{CH_2}$Ph), 2.85 (d, J = 5.0 Hz, 3 H, $\mathbf{CH_3}$-DMF), 2.68 (d, J = 5.0 Hz, 3 H, $\mathbf{CH_3}$-DMF); 13 C NMR (125 MHz, DMSO-d6) δC: 178.3(C = S), 163.2, 162.8(C = O), 161.5, 144.3, 143.5, 137.2, 136.6, 130.3, 129.4, 128.6, 128.1, 124.7, 124.1, 118.7, 112.9, 112.2, 109.7 (Ar-**C**), 51.0(**C**$\mathrm{H_2}$Ph), 36.3, 31.3.

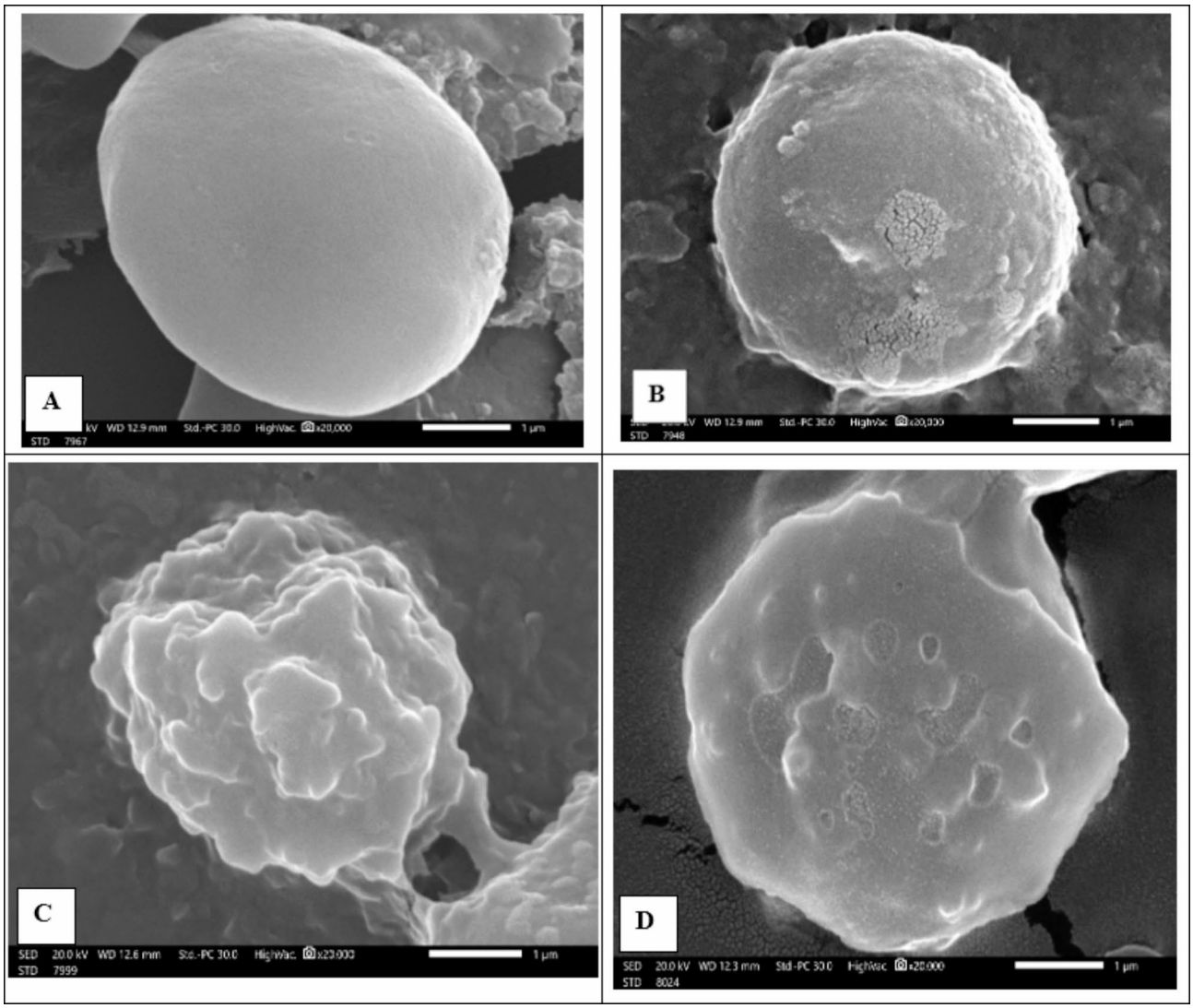

Fig. 8. Scanning electron micrographs of Cryptosporidium oocyst, (**A**) Oocyst of the infected control group (GII) revealed a spherical form with a perfectly smooth surface. (**B**) Oocysts from NTZ treated group (GIII) showed completely roughness and surface imperfections. (**C**) Oocyst from nano compound **3b** treated group showed a rough surface appearance and cyst surface abnormalities with a creation of focused blebs and deep dimples (**D**) Oocyst from nano compound **3a** treated group showed totally irregular spherical-shaped and outlines.

Preparation of Chitosan Nano-Formulation (CNPs)

Formulation of chitosan was prepared using ionic gelation method[37,38]. where half gram of chitosan was dissolved in 100 ml of 2% glacial acetic acid solution and was stirred for 2 h. Then the appropriate amount of synthesized hydrazones **3** was dissolved in 5 ml DMSO and stirred for 2 h. Following the preparation of a sodium tripolyphosphate anhydrous (TPP) solution (0.2% w/v in deionized water), the chitosan solution was vigorously stirred until equilibrium was reached, and then the thick chitosan emulsion was allowed to settle down and then subjected to centrifugation at 4,000 rpm for 30 min for CNPs **3** precipitation. For subsequent studies, the resulting precipitate was kept in sterile falcon tubes at 4 °C.

Biological evaluation

Hemolytic activity assay (cytotoxicity on RBCs)

The hemolytic activity assay is reported in the supporting information.

Drugs

The oral administration of nitazoxanide (NTZ, Alinia, Romark labs, USA) at a dosage of 100 mg/kg per day began on day 10 following infection and continued for 14 days in a row[39].

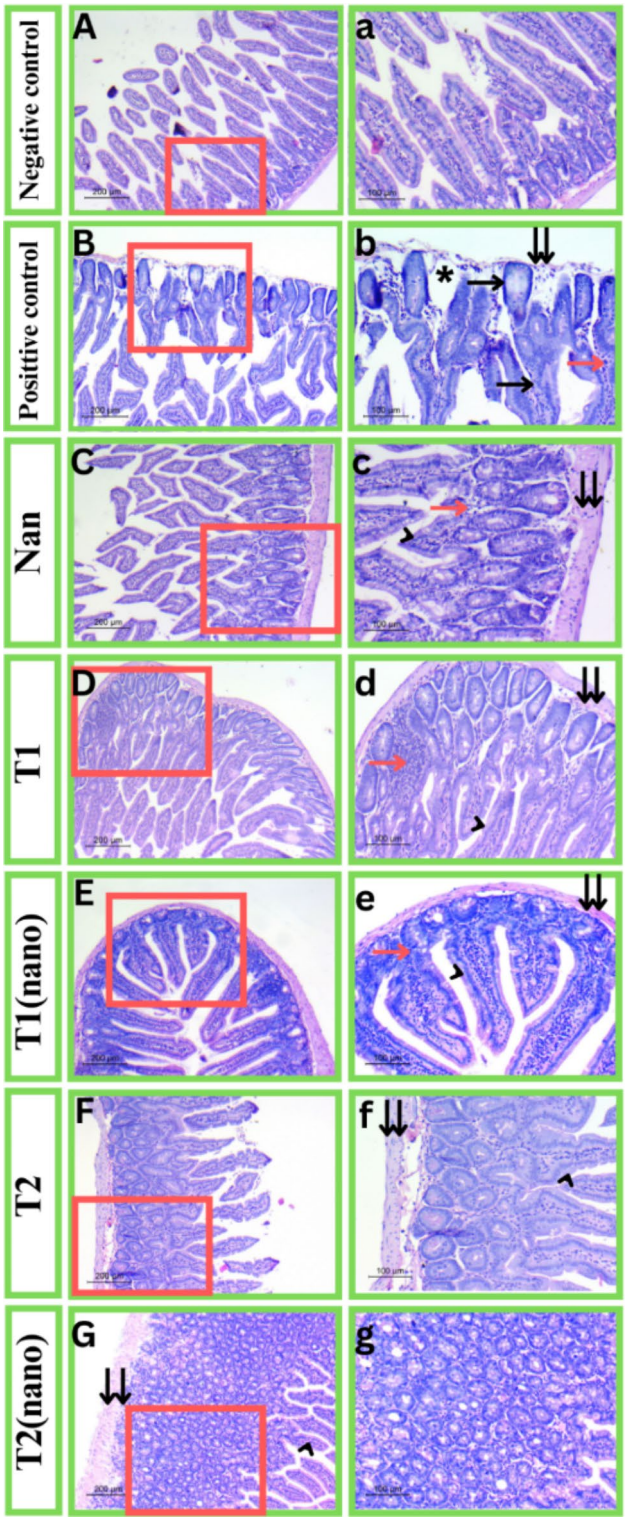

Fig. 9. histopathological changes of intestine in mice. Right panels represent a greater magnification (×200, scale bar 100 µm) of the insets in the subsequent left panels (×400, scale bar 200 µm) (H&E staining).

Oocysts Preparation

Cryptosporidium's oocysts were acquired from the Parasitology Lab, Theodor Bilharz Research Institute, Giza, Egypt. Before infection, a hemocytometer was managed to concentrate and count the oocysts in PBS solution. Five mice were given 3000–3500 oocysts intraesophageally using a tuberculin syringe to sustain the organism cycle[40,41].

Animals
This study was accomplished on 70Swiss albino male laboratory-bred mice (six-week-old, weighing approximately 20 gm). The mice were housed in regular circumstances after being acquired from Pharos University's (PUA) animal home in Alexandria, Egypt. Before being infected with Cryptosporidium, the mice were given ten days to get used to the experimental setup. Mice were housed in plastic cages with clean wood-chip bedding and enough ventilation. Every mouse was kept in a regulated environment with a temperature of 21 ± 2 ∘C and a 12-hour light/dark cycle, mice grouping details was shown in in the supporting information.

Immunosuppression
The mice's daily water intake was calculated to be around 4 milliliters, then the dexamethasone dose (0.25 mg/kg/day) was administered orally with drinking water (at a concentration of 62.5 µg/ml) for 14 succeeding days prior to infection with *C. parvum*oocysts. The immunosuppressed mice persisted in receiving the dexamethasone's dose throughout the experiment[42].

Infection
According to Rasmussen and Healey[43], the oocyst suspension (104 oocysts/mL) was made in distilled water, who stated that a mouse infection requires 104 oocysts[43].

Study design
Animals were distributed equally into Seven groups of 10 mice. At the ending of the experiment, animals were scarified to perform parasitological, ultrastructural and histopathological studies. Mice grouping details is reported in the supporting information.

Parasitological examination. Fresh fecal pellets were gathered from each mouse group on day 24, the latest day of the experiment, and labeled with the number of oocysts. For each sample was suspended in ddH2O and then homogenized. Then, made a fecal smear of 1 mg feces which was stained by the amended Ziehl–Nelsen staining method. The stained fecal smear was scanned microscopically; and the *Cryptosporidium* oocysts were calculated, the average number of oocysts per milligram of feces for every mouse was recorded for every group.
Histopathological study.
The intestines of the sacrificed animals were dissected, cleaned with saline to remove any unwanted material, and then dry out on filter paper. Before being embedded in paraffin, the specimens were divided into pieces and preserved for 24 h in 5% paraformaldehyde. The samples were break into 4 µm-thick pieces and stained with hematoxylin-eosin utilizing the standard processing methodology of Bancroft and Gamble (2008). Histopathological attributes were seen using a light microscope (Lecia, DM750 P) with a camera-equipped section examination. Furthermore, quantitative assessment was evaluated utilizing intestinal morphometric analysis.
Ethical approval and the euthanasia process:
The present experiment was accomplished in accordance with the Animal Care and Use Committee at the Faculty of Pharmacy (unit of research ethics approval committee (UREAC)), Pharos University in Alexandria (PUA 04/404/26/09/202) and was in accordance with the Animal Research: Reporting of In Vivo Experiments (ARRIVE) guidelines. The mice were given intraperitoneal injections of ketamine hydrochloride (100 mg/kg) and xylazine (10 mg/kg) to result in mice anesthesia.

Conclusion
This study portrays the design and synthesis of new formyl indole derivatives based on thiobarbituric acids **(3a** and **3b**) and their nano formulations **(NP-3a** and **NP-3b**) were designed for targeting parasitological applications. Moreover, compounds **3a** and **3b** were used for treating cryptosporidium infected mice and the results of our present study confirmed that **3a** and **3b** significantly lowered the parasite load in treated mice, particularly, **3b** had a capable therapeutic efficacy against cryptosporidiosis. Moreover, histopathological investigation of **NP-3b** treated group revealed almost normal cell architecture, which proved its efficacy and safety. The IC_{50} value was recorded to assess their cytotoxic potentials and safety profiles and the $\mathbf{IC_{50}}$ (µg/ml) results revealed a 139.13 ± 0.05 and 150.00 ± 0.03 for compounds **3a**, and **3b**; respectively. Besides, the results revealed that IC_{50} (µg/ml) = 139.13 ± 0.05 and 150.00 ± 0.03 for compounds **3a**, and **3b**; respectively. Overall, compound **3a** was found to be a promising compound in immunohistopathology; it exhibited remarkable cytotoxicity IC_{50} (µg/ml) = 139.13 within its highest zeta potential value of 29.6 mV.

Data availability
The article and its supplementary materials contain all additional pertinent data produced and examined during this investigation, including experimental, spectroscopic, and computational data. Source data are provided with this paper.

Received: 3 October 2024; Accepted: 28 November 2024
Published online: 02 January 2025

References
1. Kang, L. et al. Structure–activity relationship investigation of coumarin–chalcone hybrids with diverse side-chains as acetylcholinesterase and butyrylcholinesterase inhibitors. *Mol. Diversity*. **22**, 893–906 (2018).
2. Lu, Q. Q. et al. Nitrogen-containing flavonoid and their analogs with diverse B-ring in acetylcholinesterase and butyrylcholinesterase inhibition. *Drug Dev. Res.* **81** (8), 1037–1047 (2020).

3. Gao, X. H. et al. Structure–activity study of fluorine or chlorine-substituted cinnamic acid derivatives with tertiary amine side chain in acetylcholinesterase and butyrylcholinesterase inhibition. *Drug Dev. Res.* **80** (4), 438–445 (2019).
4. Taha, M. et al. Synthesis, α-glucosidase inhibitory activity and in silico study of tris-indole hybrid scaffold with oxadiazole ring: as potential leads for the management of type-II diabetes mellitus. *Bioorg. Chem.* **74**, 30–40 (2017).
5. Dvořák, Z., Sokol, H. & Mani, S. Drug mimicry: promiscuous receptors PXR and AhR, and microbial metabolite interactions in the intestine. *Trends Pharmacol. Sci.* **41** (12), 900–908 (2020).
6. Hu, W. et al. Update of indoles: promising molecules for ameliorating metabolic diseases. *Biomed. Pharmacother.* **150**, 112957 (2022).
7. Tan, C. et al. Antihypertensive activity of indole and indazole analogues: a review. *Arab. J. Chem.* **15** (5), 103756 (2022).
8. Comai, S. et al. Tryptophan in health and disease. *Adv. Clin. Chem.* **95**, 165–218 (2020).
9. Polyzos, K. & Ketelhuth, D. The role of the kynurenine pathway of tryptophan metabolism in cardiovascular disease. *Hämostaseologie* **35** (02), 128–136 (2015).
10. Mangge, H. et al. Disturbed tryptophan metabolism in cardiovascular disease. *Curr. Med. Chem.* **21** (17), 1931–1937 (2014).
11. Pedersen, E. R. et al. Urinary excretion of kynurenine and tryptophan, cardiovascular events, and mortality after elective coronary angiography. *Eur. Heart J.* **34** (34), 2689–2696 (2013).
12. Wu, T. et al. Indole facilitates antimicrobial uptake in bacteria. *ACS Infect. Dis.* **8** (6), 1124–1133 (2022).
13. Metidji, A. et al. The environmental sensor AHR protects from inflammatory damage by maintaining intestinal stem cell homeostasis and barrier integrity. *Immunity* **49** (2), 353–362 (2018). e5.
14. Dorababu, A. Indole–a promising pharmacophore in recent antiviral drug discovery. *RSC Med. Chem.* **11** (12), 1335–1353 (2020).
15. Yan, W. et al. Generation of indoles with agrochemical significance through biotransformation by Chaetomium Globosum. *J. Nat. Prod.* **82** (8), 2132–2137 (2019).
16. Iacopetta, D. et al. Synthesis, anticancer and antioxidant properties of new indole and pyranoindole derivatives. *Bioorg. Chem.* **105**, 104440 (2020).
17. Rathee, P. et al. Synthesis and application of thiobarbituric acid derivatives as antifungal agents. *Cell. Mol. Biol.* **62** (141.10), 4172 (2016).
18. Dabholkar, V. V. & Ravi, D. T. Synthesis of Biginelli products of thiobarbituric acids and their antimicrobial activity. *J. Serb. Chem. Soc.* **75** (8), 1033–1040 (2010).
19. Pareek, D. et al. Synthesis of some biologically important 2-thiobarbituric acid derivatives incorporating benzothiazole moiety. *Der Pharm. Lett.* **2**, 274–283 (2010).
20. Chierotti, M. R. et al. The Richest Collection of Tautomeric Polymorphs: the case of 2-Thiobarbituric acid. *Chemistry–A Eur. J.* **16** (14), 4347–4358 (2010).
21. Brown, D., Katritzky, A. & Rees, C. Synthesis of heterocyclic compounds using carbon disulfide and their products. *Compr. Heterocycl. Chem.* **3**, 57 (1984).
22. Sachar, A. et al. *Synthesis of some novel barbituric acid and 1, 3-cyclohexanedione based condensed heterocycles*. (2009).
23. Bikker, J. A., Kubanek, J. & Weaver, D. F. Quantum Pharmacologic studies Applicable to the design of anticonvulsants: theoretical conformational analysis and structure-activity studies of barbiturates. *Epilepsia* **35** (2), 411–425 (1994).
24. Fisher, M. H. *Chemistry of Antinematodal Agents, in Chemotherapy of Parasitic Diseases*p. 239–266 (Springer, 1986).
25. Deshmukh, M. et al. Green approach for Knoevenagel condensation of aromatic aldehydes with active methylene group. *Synth. Commun.* **42** (8), 1177–1183 (2012).
26. Deotale, V. D. & Dhonde, M. G. Acid catalyzed Knoevenagel condensation of thiobarbituric acid and aldehyde at room temperature. *Synth. Commun.* **50** (11), 1672–1678 (2020).
27. Kauffman, G. B. Adolf Von Baeyer and the naming of barbituric acid. *J. Chem. Educ.* **57** (3), 222 (1980).
28. Desai, N. T., Sarkar, R. & Kang, G. Cryptosporidiosis: an under-recognized public health problem. *Trop. Parasitol.* **2** (2), 91–98 (2012).
29. Abeywardena, H., Jex, A. R. & Gasser, R. B. A perspective on Cryptosporidium and Giardia, with an emphasis on bovines and recent epidemiological findings. *Adv. Parasitol.* **88**, 243–301 (2015).
30. Khan, A., Shaik, J. S. & Grigg, M. E. Genomics and molecular epidemiology of Cryptosporidium species. *Acta Trop.* **184**, 1–14 (2018).
31. Xiao, L. et al. Cryptosporidium taxonomy: recent advances and implications for public health. *Clin. Microbiol. Rev.* **17** (1), 72–97 (2004).
32. Asadpour, M. et al. Comparative efficacy of curcumin and paromomycin against Cryptosporidium parvum infection in a BALB/c model. *Vet. Parasitol.* **250**, 7–14 (2018).
33. Checkley, W. et al. A review of the global burden, novel diagnostics, therapeutics, and vaccine targets for cryptosporidium. *Lancet. Infect. Dis.* **15** (1), 85–94 (2015).
34. Yan, Q. et al. Inhibitory effects of 5-benzylidene barbiturate derivatives on mushroom tyrosinase and their antibacterial activities. *Eur. J. Med. Chem.* **44** (10), 4235–4243 (2009).
35. Detsi, A. et al. Nanosystems for the encapsulation of natural products: the case of chitosan biopolymer as a matrix. *Pharmaceutics* **12** (7), 669 (2020).
36. Hassan, E. M. et al. Synthesis, X-ray structure, Hirshfeld, DFT Conformational, cytotoxic, and Anti-toxoplasma studies of New Indole-Hydrazone derivatives. *Int. J. Mol. Sci.* **24** (17), 13251 (2023).
37. Elnaggar, Y. S. et al. Intranasal piperine-loaded chitosan nanoparticles as brain-targeted therapy in Alzheimer's disease: optimization, biological efficacy, and potential toxicity. *J. Pharm. Sci.* **104** (10), 3544–3556 (2015).
38. Silva-Carvalho, R., Baltazar, F. & Almeida-Aguiar, C. Propolis: a complex natural product with a plethora of biological activities that can be explored for drug development. *Evidence-Based Complement. Altern. Med.* **2015** (1), 206439 (2015).
39. Li, X. et al. Long-lasting anticryptosporidial activity of nitazoxanide in an immunosuppressed rat model. *Folia Parasitol.* **50** (1), 19–22 (2003).
40. Current, W. L. et al. Human cryptosporidiosis in immunocompetent and immunodeficient persons: studies of an outbreak and experimental transmission. *N. Engl. J. Med.* **308** (21), 1252–1257 (1983).
41. Operario, D. J. et al. Correlation between diarrhea severity and oocyst count via quantitative PCR or fluorescence microscopy in experimental cryptosporidiosis in calves. *Am. J. Trop. Med. Hyg.* **92** (1), 45 (2015).
42. Rehg, J. E., Hancock, M. L. & Woodmansee, D. B. Characterization of a dexamethasone-treated rat model of cryptosporidial infection. *J. Infect. Dis.* **158** (6), 1406–1407 (1988).
43. Rasmussen, K. R. & Healey, M. C. Experimental Cryptosporidium parvum infections in immunosuppressed adult mice. *Infect. Immun.* **60** (4), 1648–1652 (1992).

Author contributions

A.R.R., M.H., and S.M.S done for the study design. W.A.A, A.R.R., and M.H. synthesized and characterize the organic compounds. A.R.R., and H.A.R. completed experimental studies. A.B., and Matti Haukka completed the X-ray data. E.A.M., and B.A.B. finished the parasitology and histopathology. A.R.R., and M.H. completed the manuscript editing. All authors review and approved the final manuscript.

Funding
The authors would like to extend their sincere appreciation to the Researchers Supporting Project (RSP2025R64), King Saud University, Riyadh, Saudi Arabia.

Declarations

Competing interests
The authors declare no competing interests.

Additional information
Supplementary Information The online version contains supplementary material available at https://doi.org/10.1038/s41598-024-81683-6.

Correspondence and requests for materials should be addressed to A.R.R., S.M.S. or M.H.

Reprints and permissions information is available at www.nature.com/reprints.

Publisher's note Springer Nature remains neutral with regard to jurisdictional claims in published maps and institutional affiliations.